DYNAMIC BEHAVIOUR OF DIRECT METAL LASER SINTERED TI-6AL-4V (ELI) UNDER HIGH STRAIN RATES IN COMPRESSION LOADING

A M Muiruri[1*], M Maringa[2], W B du Preez[3] & LM Masu[4]

[1 2 3]Department of Mechanical and Mechatronics Engineering, Central University of Technology, Free State, Bloemfontein, South Africa.
[4]Department of Mechanical Engineering, Vaal University of Technology, Vanderbijlpark, South Africa.
[1*]amos.mwangi.muiruri@gmail.com
[2]mmaringa@cut.ac.za
[3]wdupreez@cut.ac.za
[4]leonard@vut.ac.za

ABSTRACT

Deformation behaviour under dynamic compression of Ti-6Al-4V (ELI) produced through additive manufacturing in two different forms; as-built (AB) and stress relieved (SR), was investigated. Both AB and SR specimens were printed using the DMLS EOSINT M280 system. Compression tests were performed on the specimens at strain rate ranges lying between ($300s^{-1}$-$400s^{-1}$) and ($600s^{-1}$-$700s^{-1}$) using a Split Hopkinson Pressure Bar. This paper presents Scanning Electron Microscope (SEM) micrographs of the resulting fracture surfaces of the tested specimens, as well as scanned surfaces of through cuts, parallel and perpendicular to the load-direction of specimens that did not fracture, with a focus on the microstructural features peculiar to shear and adiabatic deformation.

1. INTRODUCTION

Ti-6Al-4V is an α+β titanium alloy. It has been used extensively for structural materials in aircraft systems due to its high specific strength and excellent mechanical properties. This alloy has shown properties against armour piercing rounds superior to those of aluminium armour and is therefore employed as a material for combat vehicles [1]. Generally, the mechanical properties of this alloy are closely related to the microstructural features governed by the relative fractions of the α and β phases [2]. As-built AB, Direct Metal Laser Sintering (DMLS) Ti-6Al-4V has an α- martensitic structure resulting in a higher tensile strength but also a lower ductility in comparison with the stress relieved (SR) alloy DMLS Ti-6Al-4V, which has an α+ β structure. Rafi *et al.* [3] have shown that the martensitic transformation depends mainly on the cooling rate and is not critically affected by slight variances in the composition of the alloy. The high cooling rate of the AB DMLS Ti-6Al-4V specimens generates residual stresses in them which distorts the produced components. In order to increase the ductility and limit the distortion of the specimens, the produced specimens are normally stress relieved. This transforms the martensitic structure into an α+β phase [4]. Generally, Ti-6Al-4V contains interstitial impurity elements, which affect its mechanical properties. Moreover, the microstructure of the alloy, and therefore, its mechanical properties, are strongly influenced by its thermo-mechanical history [5]. According to Burkin and Love [6] the interstitial elements can be used to optimize the dynamic performance of the alloy. Interstitial elements per definition have atomic radii that are less than that of titanium. These elements include nitrogen, oxygen, carbon and hydrogen. Hydrogen in solution has little effect on the mechanical properties of the alloy. However, diffusion of hydrogen into the alloys leads to the formation of hydrides whose precipitation in the alloy cause hydrogen embrittlement (loss of ductility) and reduction in the stress intensity threshold for crack propagation [7]. The other detrimental effect of the interstitials is the reduction of toughness. The presence of oxygen and nitrogen in the alloy lowers its impact resistance progressively, with their increasing content [8, 9]. Hence the extra low interstitial (ELI) level of this alloy implies that the alloy contains

[*]Corresponding author
amos.mwangi.muiruri@gmail.com

very low (controlled) levels of interstitial elements and therefore enhanced ductility and toughness of the alloy.

The strain rates in most engineering applications ranges from 10^{-8} s^{-1} to 10^{4} s^{-1}. The strain rates are categorized into different domains based on the different applications. The different domains are tabulated in table.1 with their experimental setups and applications.

Table 1: Strain rates (s^{-1}) and their different applications [10].

Strain rate range	10^{-8}-10^{-4} (Creep)	10^{-4}-10^{0} Quasi-static	10^{0}-10^{2} Intermediate	10^{2}-10^{4} High strain rates	10^{4}-10^{8} Ultra high strain rates
Experimentation set up	Dead weights	Servo-hydraulic Testing machine	Drop weights/intermediate strain rate bars	Split Hopkinson Pressure Bar (SHPB)/ Kolsky	Pressure shear impact test
Application	Creep	Statically loaded materials	Low velocity impacts	Penetration, blade containment in engines	Planetary impact

Dynamic loading of materials usually refers to strain rates that are higher than 10^{2} s^{-1} and is present in many engineering applications such as projectile penetration, turbine blade containment in the engine, high speed machining and automotive crashworthiness.

Ti-6Al-4V is a lightweight high strength titanium alloy that is used extensively in the aviation and medical industries and to some extent in the motor industry. Many researchers have conducted experimental studies on the mechanical behaviour of the alloy at high strain rates as well as high temperatures. Yatnalkar [10], investigated the strain rate behaviour of Ti-6Al-4V under tension, compression and torsion. Significant strain rate dependence was reported in this work for all loading conditions studied with increases of 50, 56 and 77 percent of flow stress for compression, tension and torsion loading, respectively, for strain rates ranging from $10^{-4}s^{-1}$ to greater than $1300s^{-1}$. Results from the work of Wulf [11] displayed increasing linear stress flow-strain rate dependence for Ti-6Al-4V in compression at strain rates of $3000s^{-1}$ to $30000s^{-1}$.Lee *et al.* [12] presented the Ti-6Al-V4 data at compressive strain rates of $0.02s^{-1}$ to $1.0s^{-1}$ and at temperatures ranging from 25^{0}C to 500^{0} C. The researchers found that the yield strength increased with increasing strain rate at the same temperature but decreased with increasing temperature at similar strain rates [11, 12, 13]. They also observed that work hardening decreased as the temperatures and strain rates increased. This was attributed to thermal softening which occurred at the high temperature and high strain rates. The former is due to the natural consequence of elevated temperature while latter arises from the development of a rise in temperatures due to adiabatic heating during deformation at high strain rates.

Adiabatic shear bands (ASBs) are considered as a strain localization phenomenon of metals and alloys during high strain rate deformations [14]. They are a result of plastic instability arising from thermal softening which can overcome the effect of work hardening/strain hardening. When a material is subjected to high shearing strain due to high rates of the applied load, the external work will initiate plastic deformation in the material. Most of this external work, especially for materials with high thermal conductivity, will be dissipated as heat. This process increases the temperature of the material. But since materials are rarely pure without flaws, inhomogeneities in material form

concentration areas for plastic deformation. For high rates of loading and therefore high rates of deformation, the heat generated at these areas is more than is dissipated. This gives rise to higher temperatures in materials at such areas. The experimental results by Meyers et al. [15] indicated that the formation of the adiabatic shear bands occurs in two stages. Stage one is the instability produced by thermal softening and enhancement of the thermal assistance in the motion of dislocations. Stage two is localization due to major microstructural changes in the material as a result of thermal softening. According to Teilink *et al*. [16], failure of ductile materials is associated with the onset of localised plastic deformation along narrow shear bands. Once formed, shear bands signify imminent failure by the rapid nucleation, growth and coalescence of voids and cracks within the bands under increasing stress [13, 17]. Failure may be delayed due to the collapse of the voids formed, increasing crack friction which affects the crack growth and propagation or suppression of void nucleation. In the limit of sufficiently large confining stresses, shearing of the band eventually produces fracturing of a sample. The adiabatic shear deformation mode is generally observed in ballistic impact, explosive fragmentation, machining grinding and metal forming [18].

Dieter [19] suggested that dislocations in alloys travel from one layer of the lattice to another as the shearing stresses increase. Dislocations are normally obstructed in their movements by atoms of the alloying elements or points defects, by stationary dislocations and grain defects. More force is required to overcome this obstruction. With further increase in stress the dislocation may get curved inward, ultimately transforming into a ring dislocation and a new dislocation forms at the initial point of the dislocation. Dieter further explained that plastic deformation creates a large number of dislocations and hence higher forces are required for plastic deformation. This explains the increase in strength during plastic deformation which is called strain hardening or work hardening.

Ti-6Al-4V is a material that exhibits failure due to adiabatic shear banding because it possesses the properties of high strength and low thermal conductivity [20, 21].Timothy [20] studied the structures of ASBs in the Ti-6Al-4V alloy resulting from ballistic impact. Metallographic examination of well-developed shear bands by the authors showed that they consisted of zones of intense shearing distortion of the original microstructure, modified by the elevated temperatures arising due to the applied high strain rates [20, 13]. Shear bands in an α + ß microstructure were noted by the authors to consist of a distributed ß phase within an α matrix whose characteristic differed from those of adjacent un-deformed α-grains. In the study, the microstructure at the shear zones for the acicular martensite alloy appeared in a tempered form, which is different from the original microstructure. However, it was observed in this work that there was no clear evidence in this alloy to show that the shear bands in α + ß microstructure had undergone a martensitic phase transformation.

It is evident from the foregoing material that, the mechanical properties of the Ti-6Al-4V alloy vary significantly with strain rates. Moreover, studies have shown that the rate dependence effect becomes particularly pronounced at higher strain rates [11, 12, 21]. Use of static properties in analysis and design of structures which undergo dynamic loading can on one hand lead to a very conservative overweight design or lead to designs which fail prematurely or unexpectedly. The use of dynamic properties will ensure the design of Ti-6Al-4V (ELI) structures that are weight efficient and structurally sound when subjected to dynamic loading.

This paper seeks to examine the effect of high strain rates in compression and to study the resulting failure surfaces in order to identify any possible changes in microstructure of the Ti-6Al-4V (ELI). Through cuts in directions perpendicular and parallel to the direction of application of load are used to produce surfaces whose microstructures are studied in search of critical high shear and adiabatic deformation features. Future related work will be carried out to develop initial solutions for the strain hardening exponent and constants for the existing constitutive models such as the Johnson Cook and Cowper-Symonds, which are used to predict the response of materials at high strain rates.

2. MATERIALS AND EXPERIMENTAL PROCEDURE

2.1 Material

Ti-6Al-4V (ELI) powder complying with the ASTM F3001-14 supplied by TLS Technik GmbH was used for manufacturing of the samples for high strain rate compression testing. The chemical composition of the powder used to build the specimens used in this work is shown in the Table 2.

Table2: Chemical composition of TLS Technik GmbH Ti-6Al-4V ELI alloy powder (wt. %)

Materials	Al	V	Fe	C	O	N	H	Ti
Wt. %	6.34	3.944	0.25	0.006	0.082	0.006	0.001	Bal

Ti-6Al-4V specimens were produced by the DMLS EOSINT M280 system. A back-and-forth raster scanning pattern with varying angles for each pass was used in the production of specimens. The substrate and powder materials were similar in chemical composition. Argon gas was used as a protective inert atmosphere. Of the 32 unpolished specimens manufactured for use in compression testing, half were used in the AB and the remainder taken through a stress relieve heat treatment in argon Gas atmosphere at 650^0C, with a soaking period of 3hours, thus reference to them as Stress Relieved (SR) specimens. Both the AB and SR specimens consisted of α'phase (acicular martensitic structure) as is evident from the two micrographs shown in Figure 1. This also is consistent with the work of Moletsane *et al.*[22] who showed that this regime of stress relieve heat treatment did not alter the microstructure of the Ti6Al4V (ELI).

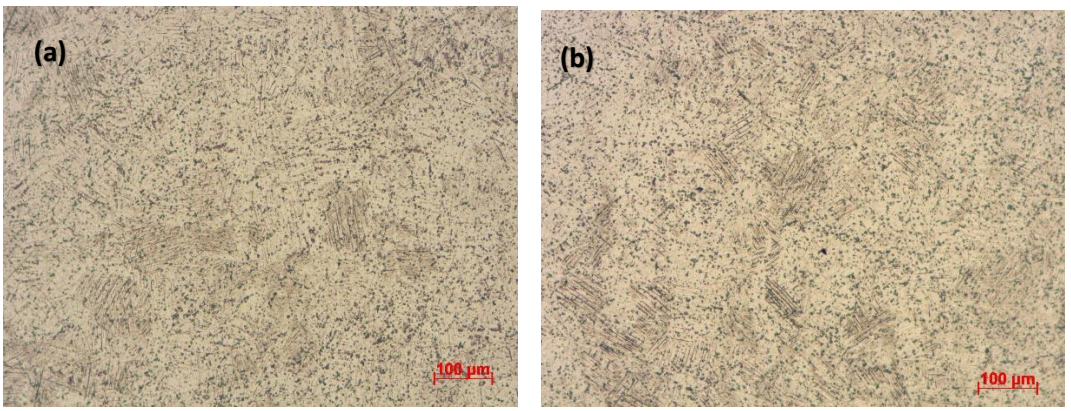

Figure 1. The Optical micrographs of (a) the as-built (AB) and (b) stress relieved (SR) samples for the transverse section of the build direction.

The compression specimens were cylindrical in shape with a nominal diameter of 6mm and a height of 12mm as per the specification of the SHPB apparatus in the Department of Mechanical Engineering, Blast Impact and Survivability Research Unit (BISRU) of the University of Cape Town that was used to conduct the test reported on here. The specifications required a height to diameter ratio of at most 2 to be used in order to facilitate dynamic stress equilibrium [23]. The tolerance on the diameters is not critical, but the ends were required to be flat and parallel within a tolerance of 0.02mm. This tolerance was achieved by facing off the two ends of the specimens on a lathe machine. This tolerance was set in order to ensure close contact between the specimen and the pressure bars of the SHPB apparatus during impact loading. To reduce the friction at the free ends of the specimens and maintain uniaxial compression in the test samples when mounted in the SHPB test equipment, molybdenum disulphide grease was used to lubricate the interface between the pressure bars and the specimen.

2.2 Experimental Procedure

A standard Split Hopkinson Pressure Bar (SHPB) was used to realize the high test strain rates required. The incident and the transmitter bars of the SHPB apparatus used for compression testing were made of steel, each with a length and diameter of 3000 mm and 20 mm, respectively. A momentum trap at the end of the transmitter bar was used as an energy damping material to bring

the bars to rest at the end of each test cycle. The setup of the SHPB test bench is shown in Figure 2.

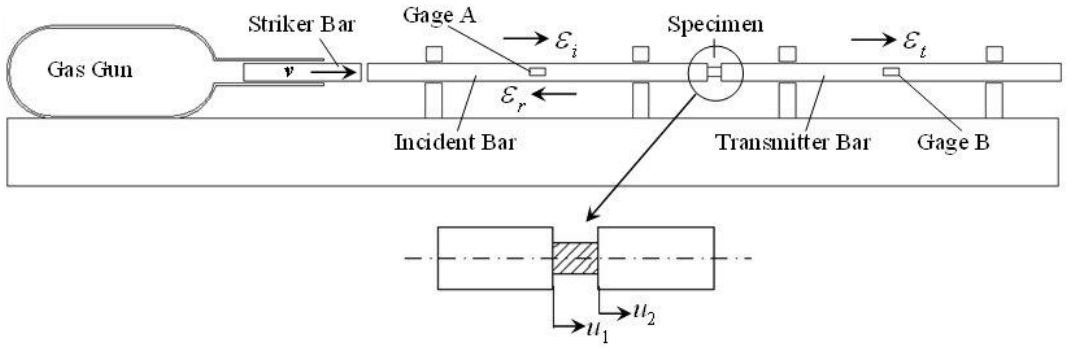

Figure 2: Schematic representation of the SHPB for compression testing

During testing the specimens were sandwiched coaxially between the incident and transmitter bars, and the incident bar was then impacted by the strike bar. The 710mm long and 20mm diameter steel striker bar was fired into the incident bar at velocities in the range of (10-11m/s) by triggering the gas gun at a pressure of 3.5 bar. This resulted in the generation of a compressive wave that propagated along the incident bar until it reached the input interface with the specimen. At this point part of the wave was reflected back along the incident bar, while the other part was transmitted through the specimen and into the transmitter bar.

The incident pulse (ε_i) was produced in the incident bar through the striking action of the striker bar moving at a velocity (10-11m/s) onto it. The test specimen experienced high strain rate deformation under the action of the stress pulse imposed on it by the incident bar of the SHPB equipment. The strike action resulted in the generation of a reflected pulse (ε_r) in the striker bar and a transmitted pulse (ε_t) in the specimen and transmitter bar. These pulses are shown in the Figure 3. An ADLINKPCI-9812 high-speed data acquisition card was used to record the voltage time signal for the incident, reflected and transmitted waves during the deformation process where the pulses were sampled at a frequency of 20MHz and at a 12-bit resolution, and stored as a TEXT files.

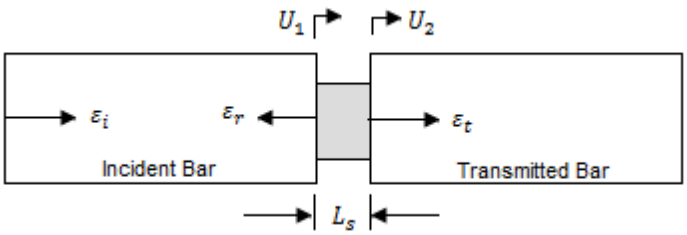

Figure 3: Schematic diagram of the pulse in the compressive (SHPB) incident, specimen and transmitter bars.

During the experiment, the test under each strain rate range was repeated seven times and the stress, strain and strain rate data captured, in all instances, averaged in order to enhance its credibility. Generally the SHPB experiment is associated with uncertainties of dispersion and effect of friction which affect the recorded pulse leading to spuriously results [24]. The variability of data obtained is not addressed here as the present work focuses on the fracture surfaces and the wire cut surfaces of the un- fractured specimens. The dimensions of each specimen were measured carefully and recorded prior to testing in order to detect differences due to fabrication. In order to obtain two strain rates regimes under the compression testing, the lengths of the specimens were varied. 12mm and 6mm long specimens were used for testing at strain rates in the ranges (300s-1-

400s-1) and (600s-1-700s-1), respectively. Based on the assumption that the elastic wave propagated in the incident, specimen and transmitter bars was one-dimensional, the strain (ε), strain rate ($\dot{\epsilon}$), and the flow stresses (σ) in the specimen were calculated using the reflected wave pulse (ε_r) and the transmitted wave pulse (ε_t) in accordance with the following formulae [25]:

$$\varepsilon(t) = \frac{-2C_0}{L}\int \varepsilon_r dt \quad (1)$$

$$\dot{\epsilon}(t) = \frac{-2C_0}{L}\varepsilon_r \ = \frac{v_i - v_t}{l_s} \quad (2)$$

$$\sigma(t) = \frac{EA}{A_S}\,\varepsilon_t(t) \quad (3)$$

Where C_0 is the longitudinal wave velocity in the incident and the transmitted bars, L is the effective gauge length of the specimen, E is the Young's modulus of the incident and the transmitted bars, A and A_s are the cross-sectional areas of the bars and the specimen, respectively.

3. EXPERIMENTAL RESULTS AND DISCUSSION

3.1 Microstructural observation of Micrographs

The test samples were examined using an optical microscope and a scanning electron microscope (SEM) in order to determine the deformation behaviour of the specimens upon imposition of dynamic compression on them. While all tested specimens showed deformation, the results shown in Table 3 demonstrate that 14%AB and 29%SR failed for testing conducted in the range ($300s^{-1}$-$400s^{-1}$) while 42%AB and 71 %SR failed for testing conducted in the range ($600s^{-1}$-$700s^{-1}$). It is evident,that a higher number of specimens fractured at the higher testing range.

Table 3: Conditions of the specimens after dynamic compression testing.

Specimens.	**As Built.**		**Stress Relieved.**	
Strain Rates (s^{-1})	300-400	600-700	300-400	600-700
No. of Fractured specimens	1	3	2	5
No. of Un-fractured specimens	6	4	5	2
Total	7	7	7	7

The compressive fracture strength of the Ti-6Al-4V is expected to decrease as a result of stress relieving heat treatment, while the ductility is expected to improve. This was a result of the reduced residual stress in the AB microstructure [26] as a result of due heat treatment.

The un-fractured specimens tested at the lower strain rate range, were cut through using Electrical Discharge Machining (EDM) for examination in a SEM. Cutting of the specimens was done both along the axial and transverse directions of the compression load as is shown in Figure 4.

The cut specimens were mounted on plastic holders and polished using silicon carbide grinding/polishing cloth in three stages: 9μm, 3μm and 1μm. After mounting and polishing the specimens, they were etched in order to reveal the details of the microstructure. The polished metallographic specimens were etched using a solution of Kroll's reagent consisting of 97mL H_2O, 3ml HNO_3 and 1ml HF. The fractured surfaces of the AB and SR specimens were cleaned for a period of 3 minutes in an ultrasonic cleaner, using ethanol as the cleaning solvent, and then investigated on a SEM.

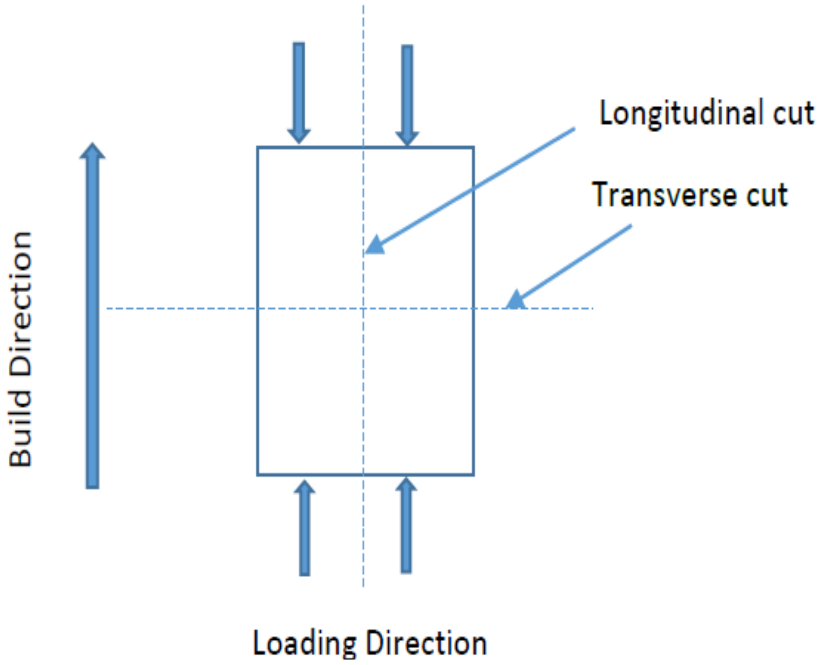

Figure 4: The orientation and cut-directions of the specimen

For compression loading in the strain rate range of (300-400) s^{-1}, the SEM micrographs of the deformed specimens is as shown in Figure 5 (a & b). The micrographs show adiabatic shear bands with the average orientations of $(40\pm10)^0$ for the SR specimens and $(50 \pm10)^0$ for the AB specimens to the axis orthogonal to the compression axis as also shown in Figure 5. The average values of the orientation were obtained from various sections along the same shear band.

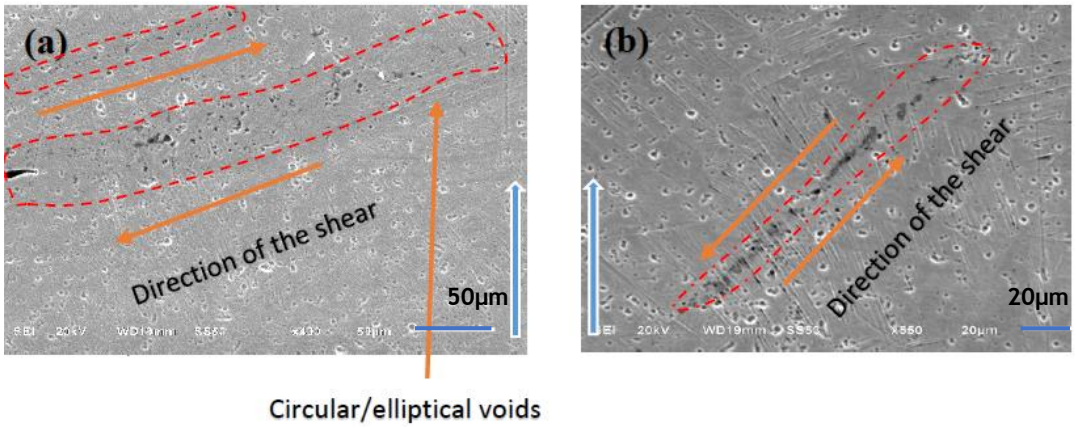

Figure 5: The longitudinal deformed microstructures of (a) SR and (b) AB viewed in the SEM, for compressive deformation at a strain rate between $300s^{-1}$ - $400s^{-1}$. The thick blue arrow on each micrographs indicates the build direction

Figure 5 reveals the presence of voids and micro cracks that appear as dark patches on the micrographs, coalescing along the shear bands. The shear bands are therefore seen to be sites in which voids formed and coalesced, which eventually leads to separation of the specimen along the

ASBs. The nucleation of voids at a section of the shear surface in which shear bands exist occurs when significant thermal softening is experienced [17, 21, 27]. The width of the shear band for the AB specimens is seen in Figure 5 to be narrower in comparison to that of the SR specimens. Measurements of the shear bands in Figures 5 (a & b) give average respective values of 20μm and 5 μm, respectively. This is consistent with the observation made by Bradley and Yilong [28] that, the width of the shear bands is greatly influenced by the material hardness; it decreases with increasing hardness of the material. Moletsane et al. [22] demonstrated that stress relieving at a temperature of 6500C and a soaking period of 3hours decreased the Vicker micro-hardness of AB specimens from an average value of 389 ±14.8HV_{300} to 374±17HV_{300}.

Figure 6 shows the occurrence and orientation of shear bands for AB and SR specimens.

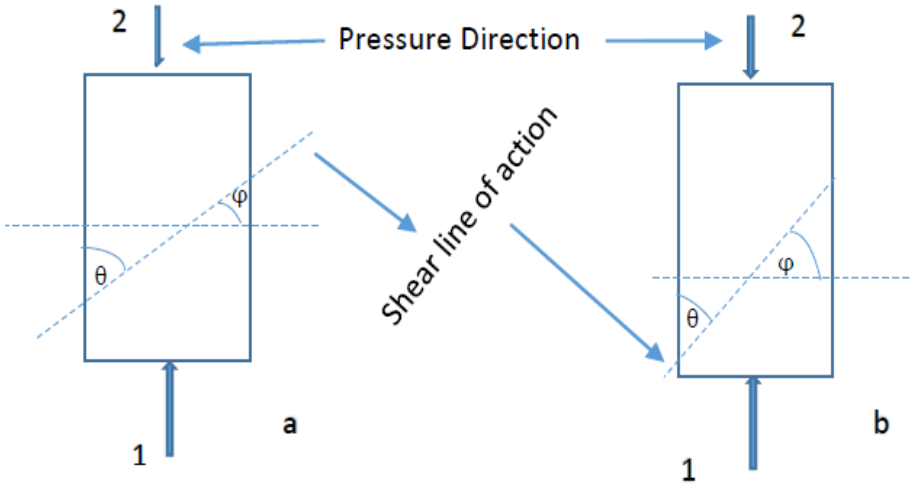

Figure 6. Schematic description of the mode of failure of (a) SR and (b) AB specimens. The numbers 1 & 2 indicate the input and output interfaces of the SHPB bars.

The locations of the shear bands for the AB and SR were found to differ along the longitudinal direction of the compressive specimens as shown in Figure 6. This is expected to be as a result of increasing magnitude of residual stresses with the height of the samples in Z-build direction [29, 30, 31]. This phenomenon will imply lower compressive stresses at on upper surfaces of AB specimens, for the same applied compressive load and therefore less likelihood for failure inducing shear bands to occur on these upper surfaces. For the two stress state ($\sigma_x = \sigma_{ec}$ and $\sigma_y = 0$) that prevails in this case, the angle of maximum shear stress ($2\theta = Tan^{-1}\left(\frac{\sigma_{ec}}{2\tau_{xy}}\right)$) is expected to decrease with decreasing values of the effective compressive stress. The effective compressive stress (σ_{ec}) in this case in the sum of the applied compressive stress (σ_c) and the residual tensile stress (σ_{rt}) in the specimen. This trend is clearly evident in Figure 6 which shows the average angle of inclination φ of the shear bands to be higher for the AB than the SR specimens; noted to be on average $(50 \pm 10)^0$ and $(40 \pm 10)^0$ for the AB and SR specimens measured orthogonal to the compression axis.

At large plastic deformations due to imposition of high strain rates such as those between $600s^{-1}$ - $700s^{-1}$, localised heating is expected to lead to localisation of the plastic flow which was reported by Bradley [21] to be a catastrophic phenomenon since it may lead to fracture by intense localized shear. Most of the fractured specimens were loaded at this higher strain rate range. The schematic description of the fracture features and orientation of the ASB as summarized in Lee's study and comparison with the fracture surfaces in this study are shown in Figure 7. Generally, compressive loading causes a transverse bulging of specimens as a result of circumferential /hoop stress that is induced along the equatorial plane of a cylindrical specimen. This creates a tensile loading state.

This explains the coexistence of the tension and the shear regions which form an X-shape on the fracture surface. Failure/fracture of the compression loaded specimens occurs along shear bands.

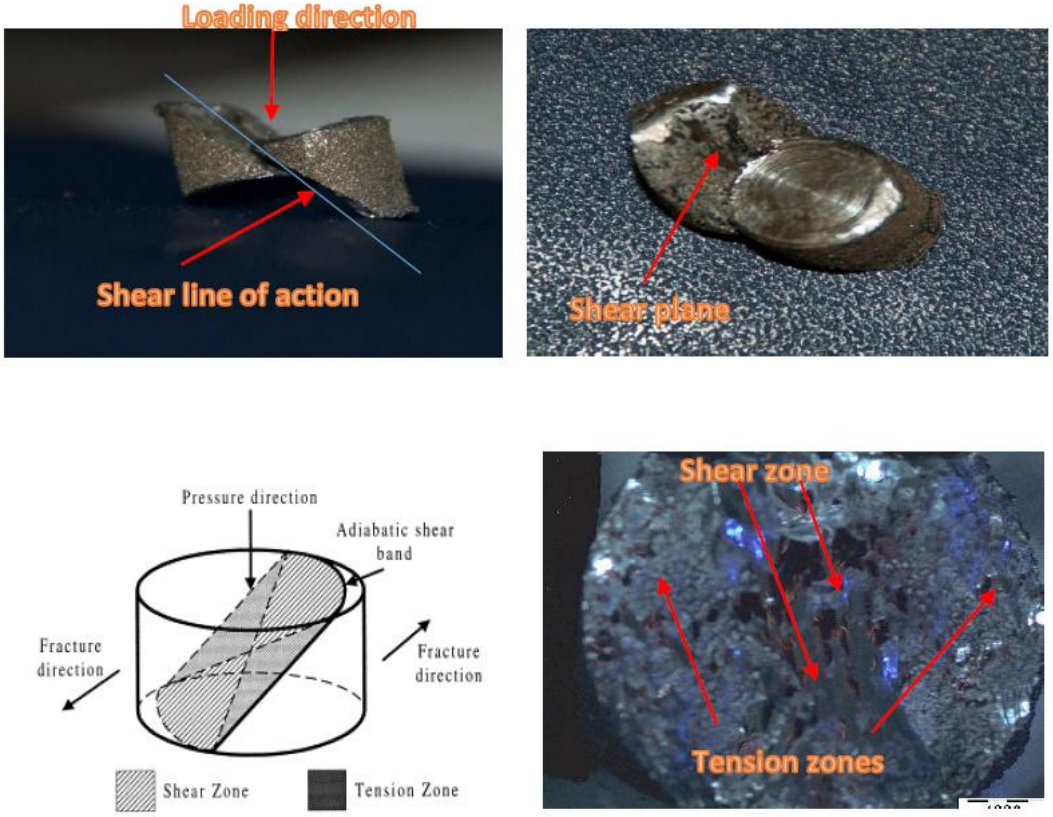

Figure 7: .Schematic descriptions and features of the fractures surface [27]

Figure 8 shows voids and cracks with different features that form within the ASB for the AB and SR specimens. As was seen in the Figure 5, voids form on the shear band. Circular or elliptical voids then coalesce along the section of the shear band. Bradley and Yilong [28] demonstrated that there exists a difference between brittle and ductile transformed shear bands. The brittle transformed shear bands are characterised by sharp cracks within the transformed sheasr band, while the ductile transformed shear bands are characterised by equiaxed voids forming along the shear bands, which then link up together to cause ductile rapture.

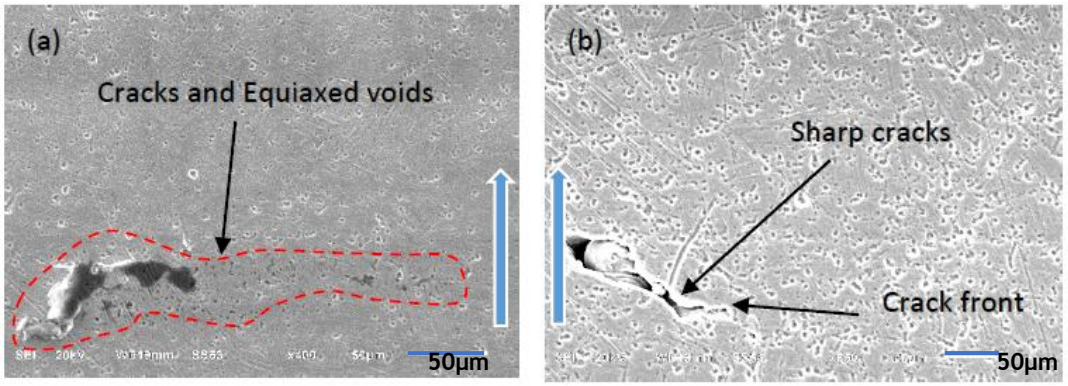

Figure 8: The growth of cracks and micro voids along the transformed band taken at different magnifications. (a) The equiaxied voids in the SR specimens noted at a magnification of x400(b) the sharp growing crack in the AB specimen noted at a magnification of x550.The blue arrows in each image indicates the build direction

The fractographs presented in Figures 5 and 8 suggest that the specimens may have failed as a result of separation along one of the formed adiabatic shear bands. Similar observation was reported by Peng *et al*. [13]. In every case it is seen that the fracture surfaces consist of two main characteristics, a relatively smooth surface and a dimple like structure corresponding to ductile fracture. The smooth surface is likely to have arisen from rubbing of opposing surfaces during shear.

Another feature that was observed along the fracture surface of most tested SR specimens was clusters of knobbly regions such as those shown in Figure 9(c). This feature may have formed as a result of (a) the local high temperatures within the shear band transforming the band into liquid, which is cooled by the surroundings almost immediately and/or (b) frictional heat produced by the two fractured surfaces subjected to shearing. These two effects alone or together make it easier for the formed dimples to deform into the features seen in Figure 9(c) during fracture.

The dimples structures seen in Figure 9 were elongated towards the direction of the shear. At the same magnification of x350 it was observed that the dimples in the SR micrograph shown in Figure 9(a) were more elongated and dense in comparison to the AB micrograph shown in Figure 9(b) which were shallower and less dense. This observed difference in the elongation of dimples is likely to be a result of the difference in ductility and strength of the two forms of specimens that were tested. The AB specimens, with their acicular martensitic microstructure are expected to have higher values of strength and lower ductility than the SR specimens.

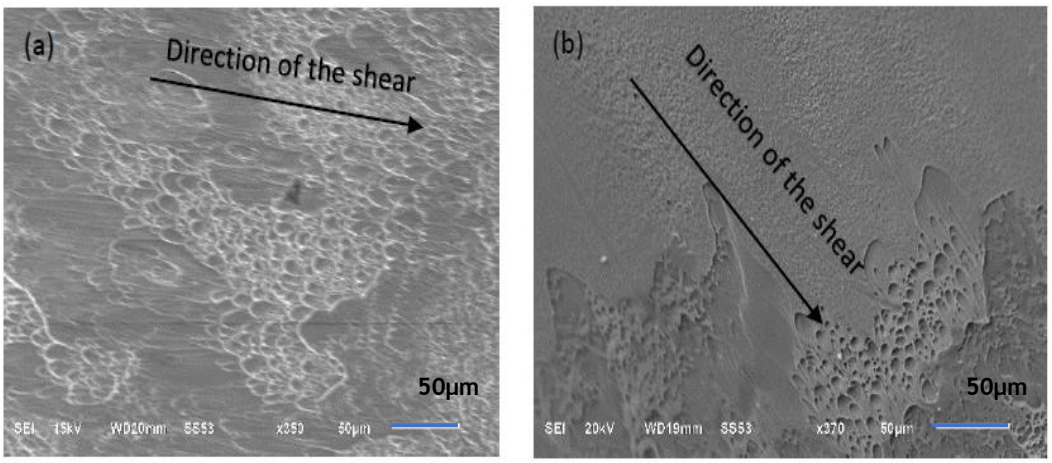

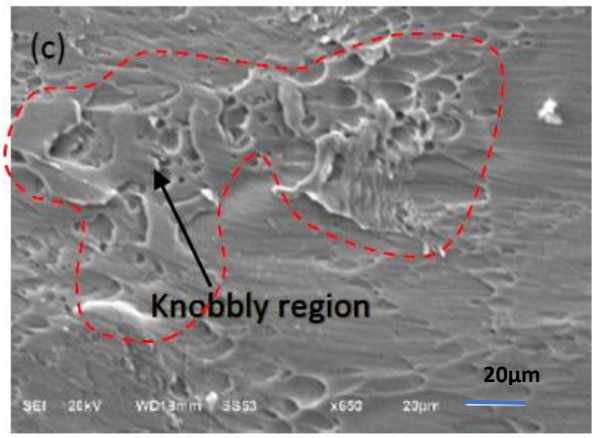

Fig 9: Scanning electron micrographs of the fracture surface (a&c) SR and (b) AB.

4. CONCLUSIONS

Compression tests of DMLS prepared Ti-6Al-4V (ELI) alloy in two different conditions AB and SR were performed to investigate the influence of the strain rates on the deformation behaviour of the material. It can be concluded from the work presented here that:

1. The adiabatic shear bands are the primary zones in which failure occurs for the two forms of the alloy.
2. The width and the morphology of the shear bands differ for the two forms of the alloy, which is known to be a result of variation in the hardness of the alloy due to stress relieving.
3. The equiaxied voids and cracks formed in the SR specimens eventually produced ductile fracture with elongated parabolic dimples as opposed to the AB specimens which produced shallower dimples. The AB samples showed a more brittle failure mode than the SR specimen.
4. The distribution of the residual stress in the AB samples has an effect on the plane of maximum shear stress, which results in the observed locations and inclinations of the ASBs. The exact distribution of the residual tensile stresses along the longitudinal axis of the specimens and therefore location and inclinations of the ASBs are the subject for further research.
5. The AB DMLS produced Ti-6Al-4V (ELI) is not suitable for application where high ductility is required. Stress relieving on the other hand improves the ductility while the strength decreases. There is a need to develop an optimum microstructure through the heat treatment of the AB samples produced through DMLS process to obtain well balanced mechanical properties such as strength and ductility. Further research is aimed at the development an optimum microstructure for dynamic loading.

REFERENCES

1. **Ogorkiwicz R.M**. 2002. Armour for light combat vehicles, *Jane's International defence review.pp41-45.*
2. **Lutjering. G & Williams**.2003.Titanium (Springer, Germany)
3. **Rafi.H.K, Karthik. N.V, Haijun Gong, Thomas L. Starr, and Brent E. Stucker**.2013 Microstructures and mechanical properties of Ti6Al4V parts fabricated by selective laser melting and electron beam melting, *Journal of Materials Engineering and Performance*, vol. 22,(12), pp. 3372-3383.

4. **Lore Thijs, Frederik Verhaeghe, Tom Craeghs, Jan Van Humbeeck, Jean-Pierre Kruth**.2010.A study of the microstructural evolution during selective laser melting of Ti-6Al-4V, *Acta Materialia*, 58, pp. 3303-3312.
5. **Montgomery, J.S., Wells, M.G.H., Roopchand, B., Ogilvy, J.W., 1997**. Low cost titanium armours for combat vehicles, JOM, 49(5), pp 45-47.
6. **Burkins,M.,Love W.** 1996. Effect of annealing temperature on the ballistic limit velocity of Ti-6Al-4V ELI, *Proceedings of the 16th International Symposium on Ballistic. San Francisco*, pp.723-732.
7. **Matthew J. Donachie.** 2000. *Titanium: A Technical Guide*, 2nd Edition pp 97-99.
8. **Jaffee, R. I., Holden, F. C., and Ogden, H. R**. 1954. Mechanical Properties of Alpha Titanium as Affected by Structure and Composition, *Journal of Metals* -' 6 1282. (21) Ogden.
9. **Holden.H.R & Jaffee, R. I**.1955.Structure and Properties of Titanium-Carbon Alloys 11, *Journal of Metals, 7*, pp 105- 112.
10. **Ravi Shriram Yatnalkar, B.E.**2010. Experimental Investigation of Plastic Deformation of Ti-6Al-4V under Various Loading Conditions. *Presented in Partial Fulfilment of the Requirements for the Degree Master of Science in the Graduate School of the Ohio State University*.
11. **Wulf.G.L**. 1976. High strain rate compression of titanium and some titanium alloys, *International Journal of Mechanical Sciences*, 21 pp: 713–718.
12. **Woei-Shyan Lee and Ming-Tong Lin**. 1995.The effects of strain rate and temperature on the compressive deformation behaviour of Ti-6Al-4V alloy.,*Journal of Materials Processing Technology*, 71:235–246.
13. **Peng-Hui, Wei-Guo, Wei-Dong, Yu Su and Xin-Lin**.2015. Thermo mechanical response of 3D laser –deposited Ti-6Al-4V alloy over a wide range of strain rates and temperatures, *Material Science and Engineering*: A 647, pp: 34-42.
14. **Mohammadhosseini, Massod, Fraser and Jahedi** .2015. Dynamic compressive behaviour of Ti-6Al-4V alloy processed by electron beam melting under high strain rate loading. *Adv. Manuf*. 3 pp:232–243
15. **Meyers MA, Subhash G, Kad BK, Prasad L**.1994 Evolution of microstructure and shear-band formation in a-hcp titanium, *Mech Mater*. 17 pp: 83-175.
16. **Teirlink,D.Zok,F**. Embury, J.D. and Ashby, M.F.,(**1988**),Fracture Mechanism Maps in Stress Space, *Acta Metall*,36 pp:1213-1228.
17. **Biswas, Ding, Field and Bandyopadhyay**. 2012. Deformation and fracture behaviours of laser processed dense and porous Ti-6Al-4V alloy under static and dynamic loading. *Material Science and Engineering: A* 549 pp: 213-221.
18. **Liao SC, Duff J**. 1988. Adiabatic shear bands in a Ti–6Al–4V titanium alloy, *J Mech Phys Solids*. 46(11),pp:2201-2231
19. **G. Dieter**.1986. *Mechanical Metallurgy*, SI ed., Mc Graw Hill.
20. **Timothy SP**. 1987. The structure of adiabatic shear bands in metals, *A critical review*. *Acta Metall*. 35(2), pp: 301-306.
21. **X. Li, C. Wang, W. Zhang, and Y. Li**.2009.Fabrication and characterization of porous Ti6Al4V parts for biomedical applications using electron beam melting process, *Materials Letters 63(3-4), pp. 403-405*.
22. **Molestsane, Krakhmalev, Du Plessis, Yadroitsava, Yadroitsev and Kazantseva,** 2016. Tensile properties and microstructure of direct metal laser-sintered Ti-6Al-4V (ELI) alloy. *South African Journal of Industrial Engineering November 2016 Vol 27(3) Special Edition, pp 110-121*.
23. **Noori S. Al-Maliky**. 2014. Dimension effect on dynamic stress equilibrium in SHPB tests. *International Journal of Materials Physics. 5 (3),* pp: 15-26.
24. **L.D. Bertholf, C.H. Karnes.** 1975. Two dimensional analysis of the split Hopkinson pressure bar system, *J. Mech. Phys. Solid*s 23, 1–19
25. **Gray III G.T**.2000. Classic split-hopkinson pressure bar testing. *ASM Handbook*, 8, pp: 462–476.
26. **Ming Yan and Peng Yu 2015.** An Overview of Densification, Microstructure and Mechanical Property of Additively Manufactured Ti-6Al-4V — Comparison among Selective Laser Melting, Electron Beam Melting, Laser Metal Deposition and Selective Laser Sintering, and with Conventional Powder Metallurgy. *http://dx.doi.org/10.5772/59275*. (28/08/2107).

27. **Lee WS, Lin CF**. 1998. Plastic deformation and fracture behaviour of Ti–6Al–4V alloy loaded with high strain rate under various temperatures. *Mater Sci Eng A*. 241(1–2), pp: 48-56.
28. **Bradley Dodd & Yilong Bai.** 2015. *Introduction to Adiabatic shear localization*. Revised Edition. Imperial College Press.
29. **Furumoto, T., Ueda, T., Aziz, A., Sanusi, M., Hosokawa, A. and Tanaka, R**. 2010. Study on reduction of residual stress induced during rapid tooling process: Influence of heating conditions on residual stress. *Key Engineering Materials*, 447-448, pp. 785-789.
30. **Mercelis, P. and Kruth**, J.-P. 2006. Residual stresses in selective laser sintering and selective laser melting,*Rapid Prototyping Journal, 12(5), pp. 254-265*.
31. **Van Belle, L., Vansteenkiste, G. and Boyer, J.-C**. 2012. Comparisons of numerical modelling of the Selective Laser Melting. *Key Engineering Materials*, 504, pp. 1067-1072.
32. **Da Silva MG, Ramesh KT**.1997. The rate-dependent deformation and localization of fully dense and porous *Ti-6Al-4V, Mater Sci Eng A Struct.232* PP: 11-22.